Nano Research
DOI 10.1007/s12274-017-1640-1
Research Article

ISSN 1998-0124
CN 11-5974/O4

Pristine mesoporous carbon hollow spheres as safe adjuvants induce excellent Th2-biased immune response

Manasi Jambhrunkar[1], Meihua Yu[1], Hongwei Zhang[1], Prasanna Abbaraju[1], Anand Kumar Meka[1], Antonino Cavallaro[2], Yao Lu[1], Neena Mitter[2] (✉), and Chengzhong Yu[1] (✉)

[1] *Australian Institute for Bioengineering and Nanotechnology, The University of Queensland, Brisbane, QLD 4072, Australia*
[2] *Queensland Alliance for Agriculture and Food Innovation, The University of Queensland, QLD 4072, Australia*

Received: 15 January 2017
Revised: 1 April 2017
Accepted: 8 April 2017

KEYWORDS

invaginated mesoporous carbon hollow spheres,
adjuvant,
ovalbumin,
vaccine,
immune response

ABSTRACT

The development of a safe and effective adjuvant that amplifies the immune response to an antigen is important for vaccine delivery. In this study, we developed pristine mesoporous carbon hollow spheres as high-capacity vaccine protein nanocarriers and safe adjuvants for boosting the immune response. Mono-dispersed invaginated mesostructured hollow carbon spheres (IMHCSs) have an average particle size of ~200 nm, large pore size of 15 nm, and high pore volume of 2.85 $cm^3 \cdot g^{-1}$. IMHCSs exhibited a very high loading capacity (1,040 $\mu g \cdot mg^{-1}$) towards ovalbumin (OVA, a model antigen), controlled OVA release behavior, excellent safety profile to normal cells, and high antigen delivery efficacy towards macrophages. *In vivo* immunization studies in mice demonstrated that OVA-loaded IMHCSs induced a 3-fold higher IgG response compared to a traditional adjuvant QuilA used in veterinary vaccine research. OVA delivered by IMHCSs induced a higher IgG1 concentration than IgG2a, indicating a T-helper 2 (Th2)-polarized response. Interferon-γ and interleukin-4 concentration analysis revealed both T-helper 1 (Th1) and Th2 immune responses induced by OVA-loaded IMHCSs. IMHCSs are safer adjuvants than QuilA. Our study revealed that pure IMHCSs without further functionalization can be used as a safe adjuvant for promoting Th2-biased immune responses for vaccine delivery.

1 Introduction

Vaccines aim to induce effective long-term immune response towards specific antigens and provide protection against diseases [1]. Recombinant/subunit vaccines are safer alternatives for use in attenuated vaccines with reduced side effects compared to older-style live or killed whole organism vaccines [1, 2]. However, the immunogenicity imparted by these vaccines is relatively low, and thus exogenous adjuvants are used to enhance the immune response [3]. Incorporation of adjuvants in the vaccine formulation

Address correspondence to Chengzhong Yu, c.yu@uq.edu.au; Neena Mitter, n.mitter@uq.edu.au

also helps to achieve qualitative T-helper 1 (Th1) and T-helper 2 (Th2) responses [4]. Th1 cells induce cell-mediated responses by affecting cytokines such as interferon (IFN)-γ, whereas Th2 cells provide humoral and mucosal immunity through cytokines such as interleukin (IL)-4 [5]. Both Th1 and Th2 responses are required for efficient activation of an immune response [4].

Since 1920, various adjuvants have been studied, including Alum, Freund's adjuvant, QuilA, and lipopolysaccharides [6, 7]. Most of these adjuvants exhibit toxicity and cause local allergies [8–10]. In recent years, nanoparticles have attracted attention as nanocarriers and self-adjuvants [11, 12]. Encapsulation of antigen proteins in a nanocarrier can improve the delivery efficacy of antigens to antigen-presenting cells (APCs) [13], extend the antigen release profile, and enhance the levels of immune response [14]. Nanoparticles such as liposomes, chitosan, virus-like particles, layered double hydroxides, carbon, poly(lactic-co-glycolic acid) (PLGA), and mesoporous silica nanoparticles have been reported as effective adjuvants for improving the immune response of ovalbumin (OVA), a model antigen protein [15–20]. However, these particles lack high antigen loading [15, 21]. This limitation can be partially circumvented by surface hydrophobicity modification of nanoparticles, which improves antigen loading capacity and sustained release behavior, antigen uptake by macrophages, and eventually the immune response [13, 22, 23]. Nevertheless, the introduced hydrophobic groups lead to increased toxicity [24]. It remains a challenge to develop nanoparticle-based adjuvants with a large antigen loading capacity, high safety profile, and excellent adjuvant effects to stimulate an immune response.

Carbon nanoparticles with intrinsic hydrophobicity have widespread bio-applications [25, 26]. Carbon nanotubes (CNTs) are the most commonly studied carbon materials with demonstrated adjuvant effects [27]. However, CNTs cannot load proteins inside the channel because of their small size, and thus vaccine proteins are generally attached to the outer surface of CNTs using coupling agents [25, 28] with limited antigen levels [27]. As the protein is not loaded inside the channel, it is still exposed to degrading enzymes, causing instability issues [27]. Recently, mesoporous carbon nanoparticles (MCNs) have attracted attention in cellular delivery [29, 30]. However, there are no reports of using MCNs as high-capacity antigen protein carriers and effective adjuvants for vaccine delivery. We previously reported the synthesis of mesostructured hollow carbon spheres (MHCSs) with invaginated and intact morphologies with a high protein loading capacity [31]. Invaginated MHCSs (IMHCSs) exhibited higher hemocompatibility compared to the intact structure [31]. The recent progress in the synthesis of MCNs encouraged us to explore the potential of IMHCSs as an adjuvant in vaccine delivery.

In the present study, we evaluated the application of IMHCSs as an adjuvant for the delivery of an antigen protein OVA. IMHCSs showed high loading towards OVA (Fig. 1). OVA-loaded IMHCSs exhibited enhanced uptake in APCs, which induced the activation of co-stimulatory molecules (CD40, MHCII) expressed on the surface of maturized APCs. *In vivo* mouse studies showed that OVA-loaded IMHCSs induced a 3-fold higher IgG response compared to a traditional adjuvant QuilA.

Moreover, IMHCS-OVA induced a higher IgG1 concentration than IgG2a and high IL-4 secretion, suggesting a Th2-polarized immune response. Our results demonstrate that pure IMHCSs can be used as a safe adjuvant for vaccine delivery.

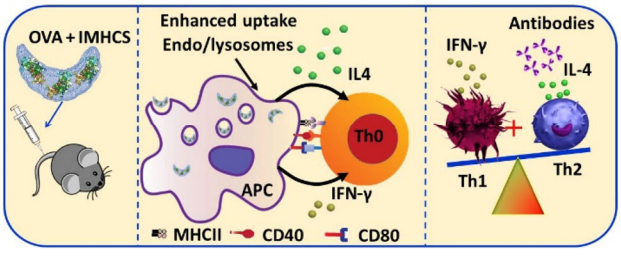

Figure 1 Schematic illustration of OVA-loaded IMHCSs with enhanced uptake in APCs and higher secretion of IL-4 compared to IFN-γ causing a Th2-biased response.

2 Experimental

2.1 Chemicals

Tetraethylorthosilicate (TEOS), resorcinol, OVA, formalin (37 wt.%), CNT, 3-[4,5-dimethylthiazol-2-yl]-2,5-diphenyltetrazolium bromide (MTT), bovine serum

albumin (BSA), fluorescein isothiocyanate (FITC), OVA tagged with FITC (OVAF), ethylene diamine tetra acetic acid, and dimethyl sulfoxide were purchased from Sigma-Aldrich (St. Louis, MO, USA). Ammonia aqueous solution (28 wt.%) and hydrogen fluoride were from Merck Laboratories (Kenilworth, NJ, USA). Ethanol was received from RCI Labscan, Ltd. (Bangkok, Thailand). QuilA was supplied from Superfos Biosector (Vedback, Denmark). Penicillin, streptomycin, phosphate-buffered saline (PBS), and Dulbecco's Modified Eagle's medium (DMEM) were from Gibco Invitrogen Corporation/Life Technologies (Carlsbad, CA, USA). Fetal bovine serum (FBS) was obtained from Moregate Biotech (Bulimba, Australia).

2.2 Synthesis of IMHCSs

IMHCSs were synthesized as described previously [31]. In a typical synthesis, 2.8 mL TEOS, 0.4 g resorcinol, and 0.56 mL formalin (37 wt.%) were added to a solution containing 70 mL ethanol, 10 mL deionized water, and 3.0 mL ammonia aqueous solution (28 wt.%) while stirring at 25 ˚C. The reaction solution was stirred for 6 h, followed by a second addition of 1.5 mL of TEOS and additional stirring for 24 h. The solid product was collected by centrifugation at 48,380*g* for 15 min, washed twice with ethanol, and dried at 50 ˚C overnight. The dried product was carbonized at 700 ˚C under a N_2 atmosphere for 5 h, followed by 5% hydrogen fluoride etching treatment to remove the silica. Finally, IMHCSs were obtained after washing twice with water and drying in air.

2.3 Characterization

The morphology of IMHCSs and CNTs was observed using a transmission electron microscope (TEM) (JEOL 1010, Tokyo, Japan) operated at 100 kV. The samples were prepared by drying ethanol-sample dispersion on copper grids. Scanning electron microscopy (SEM) images were recorded on a field emission scanning electron microscope (FESEM, JEOL 7001) operated at 10 kV. Nitrogen adsorption–desorption isotherms were measured at 77 K by using a Micromeritics Tristar II system (Norcross, GA, USA). The samples were degassed at 180 ˚C overnight on a vacuum line. The Brunauer–Emmett–Teller (BET) method was utilized to calculate the specific surface area. Pore size distribution curves were derived from both the adsorption and desorption branches of the isotherms using the Barrett–Joyner–Halanda method. Total pore volume was calculated from the amount adsorbed at a maximum relative pressure (P/P_0). Dynamic light scattering (DLS) measurements were carried out at 37 ˚C on a Malvern Nano ZS Zetasizer instrument (Malvern, UK) using ethanol, PBS (pH 7.4), and DMEM supplemented with FBS (10%), L-glutamine (2%), penicillin (1%), and streptomycin (1%) as solvents.

2.4 OVA adsorption on IMHCSs and CNTs

OVA was adsorbed onto IMHCSs or CNTs by mixing 2 mg of OVA with 1 mg IMHCS or CNT in 1 mL PBS (pH = 7.4). The mixtures were placed in a shaker at 200 rpm for 24 h at 4 ˚C. The supernatant was collected by centrifugation at 15,000 rpm for 15 min and then analyzed using a Bicinchoninic Acid assay kit (BCA, Pierce, Rockford, IL, USA). The adsorption capacity of OVA was calculated based on the original and residual concentrations remaining in the supernatant. All experiments were performed in triplicate. OVA adsorption capacity was calculated using the following equation

OVA adsorption capacity ($mg \cdot mg^{-1}$) = [*C*(original OVA, $mg \cdot mg^{-1}$) – *C*(residual OVA, $mg \cdot mg^{-1}$)] × volume of mixture (mL)/*w* (IMHCS/CNT, mg).

2.5 OVA desorption from IMHCSs and CNTs

OVA-adsorbed IMHCSs or CNTs were suspended in 1 mL PBS buffer and placed in a shaker at 200 rpm and 37 ˚C. After specific time intervals, 400 μL supernatant was collected by centrifugation at 15,000 rpm for 10 min and replaced by 400 μL fresh PBS. OVA concentration in the supernatant was estimated using the BCA assay kit.

2.6 Cell culture

Cell culture reagents were purchased from GIBCO Sciences (Grand Island, NY, USA) unless otherwise specified. Human embryonic kidney 293 (HEK 293, CRL 1573) and RAW 264.7 (mouse macrophages) cells were obtained from American Type Culture Collection (Manassas, VA, USA) and Cell Bank Australia

(Westmead, Australia), respectively. The cells were maintained in a 37 ˚C, 5 % CO_2 incubator in complete DMEM. Sub-culturing was carried out every 2 days.

2.7 Cell viability assay

The cell viabilities of IMHCS-, CNT-, OVA plus QuilA-, and OVA-loaded IMHCSs were tested using HEK 293 cells. A total of 25,000 cells were seeded into each well of a 24-well plate. After 24 h of incubation, the culture medium was replaced with 1 mL OVA plus QuilA (50 + 25 μg·mg^{-1}), OVA-loaded IMHCSs (equivalent to 50 μg·mg^{-1} of OVA), CNTs (12–100 μg·mg^{-1}), and IMHCS nanoparticles (25–400 μg·mg^{-1}) suspended in serum-free DMEM. After further incubation for 24 h, the medium was removed and 1 mL fresh complete DMEM containing 10% FBS, 1% penicillin, and streptomycin was added to each well, followed by addition of 100 μL MTT PBS solution (5 mg·mg^{-1}). The plate was then placed in a 37 ˚C, 5% CO_2 incubator for 4 h before adding 1 mL dimethyl sulfoxide to each well. Supernatant solutions were collected and centrifuged for 15 min at 15,000 rpm and the absorbance for the supernatants placed in a new plate were measured at a wavelength of 570 nm using a plate reader. Untreated incubated cells were used as a control. All experiments were performed in triplicate for each group [32].

2.8 Preparation of FITC-grafted IMHCSs and CNTs

FITC was grafted onto IMHCSs and CNTs as described previously [33]. First, 25 mg IMHCS or CNT and 0.15 mg FITC were ultrasonicated in 6.5 mL anhydrous tetrahydrofuran. The resultant solution was then stirred at 30 ˚C for 2 h. The mixture was centrifuged at 15,000 rpm for 15 min. The IMHCS and CNT labeled with FITC were further washed with PBS solution several times. Absorbance of the supernatant and washing medium was measured by ultraviolet–visible (UV–Vis) spectroscopy, which showed negligible readings in both particle systems, suggesting that all FITC had attached to the nanoparticles.

2.9 Cellular uptake of IMHCS-F and CNT-F

Cellular uptake studies for IMHCSs and CNTs were carried out by tagging the nanoparticles with FITC and OVAF-loaded nanoparticles [33]. A total of 2.5 × 10^5 RAW 264.7 cells per well were seeded into a 12-well plate. After 48 h of incubation, 10 μg FITC-tagged nanoparticles was added to each well and incubated for 2 h in a 37 ˚C, 5% CO_2 incubator. After removing the supernatant, the cells were washed twice with sterile PBS and collected. The harvested cells were washed twice with sterile PBS and then suspended in the FACS buffer (500 mg BSA, 50 mg EDTA, and 100 mL PBS free from calcium and magnesium salts). FITC uptake in the cells was analyzed using FACS BD LSR II Analyzer (BD Biosciences, Franklin Lakes, NJ, USA).

2.10 Confocal microscopy

Cellular uptake was also studied by confocal microscopy on RAW 264.7 cells. A total of 1 × 10^6 cells was adhered onto a sterile microscopic coverslip at 37 ˚C for 24 h. After 24 h, the medium was replaced with serum-free medium and the cells were treated with FITC-tagged nanoparticles and OVAF-loaded nanoparticles (CNT-FITC, IMHCS-FITC). The cells were fixed with 4% formaldehyde and permeabilized with 1% BSA for 30 min. Finally, the coverslips were placed on 4′,6-diamidino-2-phenylindole, dihydrochloride (DAPI) and viewed under a 40× confocal laser-scanning microscope (LSM510META, Zeiss, Jena, Germany).

2.11 Intracellular trafficking of nanoparticles

Raw 264.7 (1 × 10^5 cells) were allowed to attach to a sterile microscopic coverslip at 37 ˚C for 24 h followed by incubation with 5 μg·mL^{-1} OVAF-loaded nanoparticles (IMHCSs and CNTs) and OVAF + QuilA for 8 h. The lysosomes were further stained with LysoTracker Red DND-99 (Thermo Fisher Scientific, Waltham, MA, USA) according to the manufacturer's instructions.

2.12 Effect of IMHCS-OVA on dendritic cell and macrophage maturation

Briefly, mice spleens were passed through a cell strainer to obtain a single-cell suspension and red blood cells were lysed using erythrocyte lysis buffer (Sigma–Aldrich). The resulting cells were seeded in a 96-well plate at a density of 2 × 10^5 cells/well in phenol-free

Iscove's Modified Dulbecco's Media (IMDM, Glutamax medium, Gibco ®, Life Technologies) supplemented with 10% FBS, 50 μM 2-mercaptoethanol (Gibco®, Life Technologies), penicillin (1%), and streptomycin (1%) (Gibco®, Life Technologies). OVA, OVA + QuilA, OVA + CNT, and OVA + IMHCS were added to the wells and incubated for 24 h. Adherent cells were scraped from the plate and incubated with Fc-block (BD Biosciences) for 20 min at 4 ˚C, centrifuged, and resuspended in buffer containing CD11c (eBioscience, San Diego, CA, USA), F4/80, CD40, CD80, and CD86 major histocompatibility class II (MHCII, BioLegend, San Diego, CA, USA) antibodies for 30 min at 4 ˚C. The cells were then centrifuged and resuspended in 0.5 mL FACS buffer (PBS, 0.02% sodium azide, 0.5% BSA) and analyzed with an LSR II flow cytometer (BD Biosciences). The fluorescence intensities of dendritic cells and macrophages treated with PBS were measured as negative controls. The cell population costimulatory for dendritic cells (CD11c)/macrophages (F4/80) and other fluorochrome markers (CD40, CD80, CD86, MHCII) were analyzed as percent (%) positive cells using flow cytometry (FACS Aria III, BD Biosciences) and the data were processed using the FlowJo software.

2.13 Animals

Naïve 8-week-old C57BL/6J female mice were purchased from the Biological Resource Facility (Brisbane, Australia). Animal studies were conducted using 5 groups with 5 mice/group. The mice were caged in high-efficiency particulate air-filtered polycarbonate cages and were given *ad libitum* access to food and water. All mice were housed in a pathogen-free environment at controlled temperature (21 ± 1 ˚C) and a 12-h/24-h light cycle was maintained. All experiments involving animals were approved by the Animal Ethics Committee, The University of Queensland (AIBN/464/14/ARC). Experiments were blinded to treatment groups. Animals were closely monitored twice daily and remained in good health for the duration of the study with no visible deleterious health effects.

2.14 Immunizations

At the onset of the experiment, mice were divided into 5 treatment groups (n = 5). Group 1 and 2 mice were injected with OVA (50 μg) plus QuilA (25 μg) and OVA (50 μg) as two positive control groups. Group 3 mice were injected with OVA-loaded IMHCS pellets (prepared as described above) equivalent to 50 μg OVA suspended in sterile saline solution. Group 4 mice were injected with IMHCS (100 μg) as a negative control group. Group 5 was again a negative control including unimmunized mice. Dose volumes of 100 μL (in 0.9% saline, Pfizer, New York, NY, USA) were administered by subcutaneous injection at the tail base using a sterile 27-gauge needle (BD Biosciences). Three injections were administered at 3-week intervals to all treatment groups. Blood was obtained from each mouse through retro-orbital bleeds using heparin coated hematocrit tubes (Hirschmann Laborgeräte, Heilbronn, Germany) before each immunization. Fourteen days after the third immunization, the animals were sacrificed and blood was collected and analyzed for antibody titers, whereas splenocytes were collected and analyzed for cytokine (IFN-γ and IL-4) concentrations.

2.15 Estimation of OVA antibody response

The OVA-specific IgG response was determined by enzyme-linked immunosorbent assay (ELISA) as previously described [16, 32]. Briefly, microtiter plates (96-well, Nunc, Maxisorb, Roskilde, Denmark) were coated with OVA antigen in PBS solution (10 μg·mL^{-1}, 50 μL) for 24 h at 25 ˚C. The coating solution was then removed and the plates were washed once with 200 μL PBS-T (1× PBS containing 0.1% Tween 20). Coated plates were blocked with BSA (5%) and skimmed milk powder (5%, Fonterra, Auckland, New Zealand) for 1 h at room temperature (RT). The plates were then washed three times with 200 μL PBS-T, after which mouse sera diluted with PBS was added in the range of 1:1.5 × 10^4–1:3 × 10^7. Unreacted antibodies from mouse sera were removed by washing with 200 μL PBS-T. The plates were further incubated with 100 μL secondary antibody, horseradish peroxidase (HRP)-linked rabbit anti-mouse IgG (Sigma-Aldrich) (1:5,000 in PBS), or HRP-linked goat anti-mouse IgG1 (Santa Cruz Biotechnology, Inc., Santa Cruz, CA, USA) (1:2,000 in PBS) or HRP-linked goat anti-mouse IgG2A (Santa Cruz Biotechnology, Inc.) (1:2,000 in PBS) for 1 h at RT. The substrate solution 3,3′,5,5′-tetramethylbenzidine

(100 μL, Life Technologies) was used for color development. Color development was stopped using 1 N HCl and the optical density was read at 450 nm using a Tecan Infinite M 200 Pro Plate reader (Männedorf, Switzerland). Titers were determined as the reciprocal of the sample dilution corresponding to three standard deviations above the mean OD value of the population of negative sera.

2.16 Isolation of murine splenocytes and enzyme-linked spot (ELISPOT) assay

Spleens were removed aseptically from the mice and placed in 5 mL of ice-cold DMEM supplemented with 10% fetal bovine serum, 20 mM 4-(2-hydroxyethyl)piperazine-1-ethanesulfonic acid, *N*-(2-hydroxyethyl)piperazine-*N*-(2-ethanesulfonic acid (HEPES buffer, pH 7.3, Sigma-Aldrich), 1 M sodium pyruvate, 1 M Glutamax, 100 U·mL^{-1} penicillin G, 100 mg·mL^{-1} streptomycin, and 0.25 mg·mL^{-1} Fungizone. The spleens were disrupted using a plunger connected to a 3-mL syringe and passed through 100-μm mesh. The resulting cells were washed three times with 5 mL DMEM and centrifuged at 2,500 rpm for 5 min at 4 °C and then resuspended in 1 mL lysis buffer (0.15 M NH_4Cl, 10 mM $KHCO_3$, 0.1 mM Na_2EDTA) for 5 min at RT. The washing steps were repeated three times with DMEM (5 mL) each. Cell pellets were resuspended in 2 mL DMEM and the cell numbers were determined by staining with 0.2% trypan blue. Cells from each mouse spleen were seeded in triplicate onto polyvinylidene fluoride ELISPOT plates precoated with monoclonal IFN-γ (Mabtech, Cincinnati, OH, USA) capture antibody or monoclonal IL-4 capture antibody (Mabtech). Next, 2.5 × 10^5 cells were incubated in complete DMEM at 37 °C and 5% CO_2 for 40 h in the presence or absence of 1 mg·mL^{-1} OVA antigen or polyclonal activator concavalin A as a positive control. IFN-γ and IL-4 ELISPOT assays were performed according to the manufacturer's instructions. The ELISPOT plates were read on an ELISPOT reader (AID ELISPOT reader, Strassberg, Germany).

2.17 IFN-γ secretion level in RAW 264.7 cells

RAW 264.7 cells were seeded into a 96-well plate at a density of 2 × 10^5 cells/well in complete DMEM supplemented with 10% FBS and 1% Penicillin and Streptomycin (PS). After incubation for 24 h, the cells were treated with OVA (10 μg)-loaded IMHCS (10 μg) and physically mixed with IMHCS (10 μg) and OVA (10 μg) or PBS (a negative control) for 48 h. Cytokine IFN-γ levels in the cells were measured using an ELISA kit according to the manufacturer's protocol.

2.18 Statistical analysis

Data are reported as the mean ± S.E.M and differences between groups were analyzed by two-way ANOVA followed by Tukey's post-test (GraphPad Software, La Jolla, CA, USA).

3 Results and discussion

IMHCSs were prepared using a sequential heterogeneous nucleation process as reported in our previous work [31]. SEM images (Fig. 2(a)) showed that IMHCSs had a uniform and invaginated spheroidal morphology. TEM images (Fig. 2(b)) depicts a bilayered and hollow internal structure of IMHCSs with a uniform outer diameter of 192.3 ± 11.3 nm. The porous nature on the wall can be directly observed in both the SEM and TEM images.

Nitrogen sorption results of IMHCSs indicated a type IV adsorption isotherm (Fig. 2(c)). The Barrett–Joyner–Halanda pore size distribution curve derived

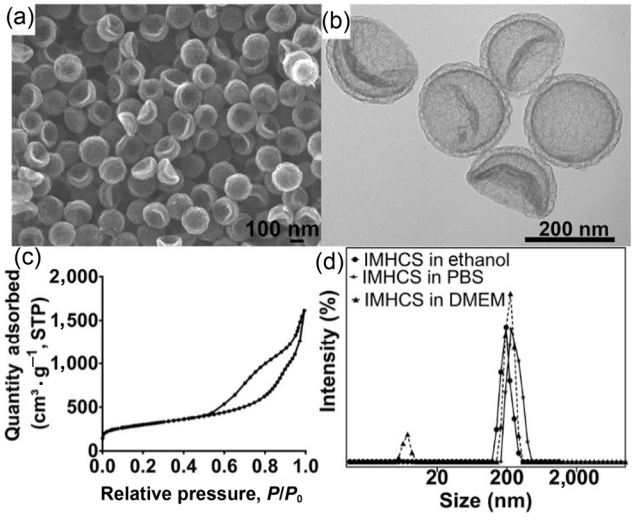

Figure 2 (a) SEM and (b) TEM images of IMHCS, (c) N_2 adsorption–desorption isotherm of IMHCS, (d) particle size distribution curves of IMHCS in ethanol, PBS, and DMEM by DLS measurement.

from the adsorption branch displays one peak centered at 15.3 nm (Fig. S1 in the Electronic Supplementary Material (ESM)), corresponding to the interlayer distance between the inner and outer layers. The pore diameter of 7.3 nm calculated from the desorption branch indicated a relatively large entrance size in the carbon shell. The BET surface area and pore volume of IMHCSs were 1,085 $m^2 \cdot g^{-1}$ and 2.85 $cm^3 \cdot g^{-1}$, respectively. To demonstrate the advantages of IMHCSs *in vitro*, commercially available CNTs (Fig. S2 in the ESM) with a pore size of approximately 2 nm, BET surface area of 138 $m^2 \cdot g^{-1}$, and pore volume of 0.93 $cm^3 \cdot g^{-1}$ (Fig. S3 in the ESM) were used.

The particle size and polydispersity of IMHCSs were further investigated in ethanol and biological media by DLS measurement. As shown in Fig. 2(d), the average particle size of IMHCSs in ethanol was 195 nm. The narrow size distribution and low polydispersity index (0.1) indicated that the particles were of uniform particle size and showed excellent dispersibility in ethanol. The hydrated diameter of IMHCSs in PBS was approximately 230 nm, which is larger than that in ethanol because of the surrounding water molecules [31]. The size distribution curve in DMEM containing 10% FBS showed two peaks at approximately 7.5 and 225 nm, attributed to FBS and IMHCS, respectively. The polydispersity index value in DMEM was relatively large (0.56) because two populations of sizes were present. Optical images of the CNT and IMHCS (Fig. S4 in the ESM) indicated that the IMHCS has better dispersibility as compared to the CNT. Numerous reports have demonstrated stronger adjuvant effectiveness of nanoparticles over those with micrometer-size in immune response amplification [13]. IMHCSs with smaller particle sizes and better dispersity may be a more potent adjuvant than CNTs.

In this study, OVA (45 kDa, 7 nm × 4 nm × 4 nm) was used as the model antigen to evaluate the adjuvant effect of IMHCSs. The loading kinetics of OVA on IMHCSs and CNTs were studied in PBS. As shown in Fig. 3(a), IMHCSs reached a high loading capacity of 1,040 $\mu g \cdot mg^{-1}$ within 10 h. In contrast, OVA adsorption reached equilibrium at 3 h for CNTs (Fig. 3(a)) with a maximum loading of 225 $\mu g \cdot mg^{-1}$, indicating that OVA was loaded mainly on the outer surface of the CNT. Compared to previously reported mesoporous carbon nanoparticles with a small mesopore size (5 nm) and low antigen loading (79 ± 4.16 $\mu g \cdot mg^{-1}$) [18], IMHCSs showed a 13-fold higher antigen-loading capacity. IMHCSs showed higher loading capacity of OVA than CNTs, silica nanoparticles [16], PLGA nanoparticles [15], and layered double hydroxide nanoparticles [17], which is attributed to the inherent hydrophobic nature of pristine carbon and unique nanostructure with a large and accessible surface area and pore volume of IMHCSs.

The sustained release of antigen from adjuvants is considered one of the main reasons for adjuvants' ability to promote an immune response [34]. It was reported that porous inorganic particles with pore sizes larger than antigens were beneficial for sustained antigen release and elicited stronger immune responses by successfully encapsulating the antigen proteins inside the pores [35]. The release behavior of OVA-loaded nanocarriers in PBS was investigated. IMHCSs displayed (Fig. 3(b)) a two-step [36] OVA release pattern with a fast release step of 50% in the first 6 h, followed by a sustained release step of 78% until 24 h. The fast release of OVA may be attributed to the OVA loaded on the outer surface of the IMHCS, and the sustained release to antigens loaded inside the interspace of two layers of the IMHCS. In comparison, CNTs showed a burst release of 100% within 2 h (Fig. 3(b)). This release pattern of OVA from pristine

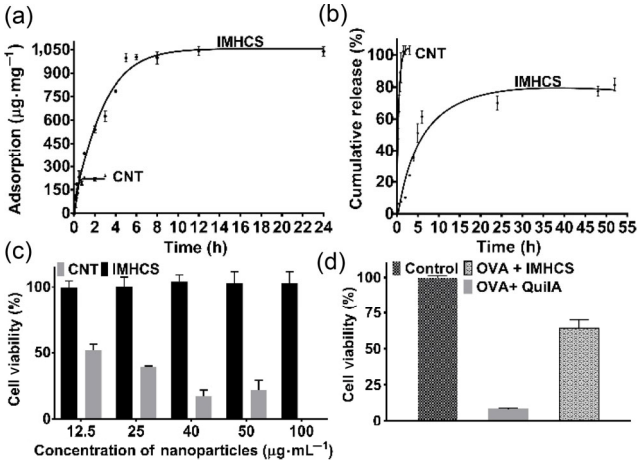

Figure 3 (a) Adsorption kinetics of OVA in PBS on IMHCS and CNT, (b) cumulative release of OVA in PBS from IMHCS and CNT, cell viability of (c) bare IMHCS and CNT and (d) OVA + QuilA and OVA + IMHCS.

CNTs further indicates that OVA was loaded only on the outer surface of the CNT with a small pore size of 2 nm. Unlike pristine IMHCSs for which controlled release can be achieved by adjusting the nanostructure and nanopores, CNTs without chemical functionalization are not suitable as nano-carriers for high loading and sustained release of OVA.

The cytotoxicity of OVA plus QuilA, OVA-loaded IMHCS, blank IMHCS, and blank CNT was tested on normal HEK 293 cells before administration to animals. The *in vitro* cell toxicity studies (Fig. 3(c)) confirmed that the blank IMHCSs showed good biocompatibility with no obvious cell toxicity over a wide concentration range (12.5–100 $\mu g \cdot mL^{-1}$), indicating excellent biosafety. The blank CNT group showed high toxicity even at low concentration of 12.5 $\mu g \cdot mL^{-1}$ (Fig. 3(c)). This observation is in agreement with literature reports suggesting that pristine CNT is toxic because of impurities or intrinsic structural defects [37]. At the same doses used in animal studies, OVA (50 $\mu g \cdot mL^{-1}$) plus QuilA (25 $\mu g \cdot mL^{-1}$) and OVA (50 $\mu g \cdot mL^{-1}$)-loaded IMHCS (50 $\mu g \cdot mL^{-1}$) exhibited 8% and 64% cell viability respectively, suggesting that the OVA-loaded IMHCS vaccine formulation is safer than OVA plus QuilA (Fig. 3(d)). This observation is in accordance with literature reports stating that QuilA induces local reactions, hemolytic effects, and systemic toxicity [38], while carbon nanoparticles have excellent biocompatibility [39, 40].

The antigens should be taken up, processed, and presented on APCs in order to generate an efficient immune response after immunization [41, 42]. Uptake of bare nanoparticles tagged with FITC was studied in RAW 264.7 cells using confocal microscopy. The feeding amount of FITC was kept constant in all groups. As shown in the confocal microscopy images (Fig. S5 in the ESM), the control without treatment showed no fluorescence. Cells with CNTs tagged with FITC (CNT-F) showed slightly higher fluorescence intensity compared to the control group. However, mono-dispersed IMHCSs tagged with FITC (IMHCS-F) showed the highest fluorescence intensity, indicating highly improved uptake performance compared to CNTs.

To further investigate the delivery performance of OVA conjugated with FITC (OVAF) using nanoparticles and QuilA in RAW 264.7 cells, OVAF was adsorbed onto the nanoparticles (CNT and IMHCS) and QuilA and uptake performance was estimated by confocal microscopy and FACS. The mass ratio of particles/QuilA to OVAF was the same in all groups. According to the FACS results shown in Fig. 4, IMHCSs are the most effective nanocarriers for delivering OVAF into RAW cells among all the groups based on mean fluorescence intensity and the percentage of positive cells. From the confocal images shown in Fig. S6 in the ESM, IMHCS also showed the highest fluorescence intensity compared to the QuilA and CNT groups, consistent with the FACS results. Thus, IMHCS with an intact carbon composition, monodispersed nanosize, and large porosity have high cellular uptake and OVA delivery efficacy [24].

The intracellular fate of the delivered protein determines the type of MHC class stimulated by the antigen. If proteins are degraded by proteasomes, MHC I protein markers will be enhanced, causing a cell-mediated response [43, 44]. If the proteins are entrapped in endosomes, they are degraded in endo/lysosomes and presented on the cell surface as MHC II antigens, which eventually helps in enhancing the antibody-mediated immune response [43, 44]. To study the intracellular fate of OVA, lysosomes were stained using Lysotracker (red) and nuclei were stained with DAPI (blue). As indicated in the confocal images (Fig. 5), OVAF plus QuilA or CNT showed small increases in green fluorescence (from OVAF) located in the lysosomes compared to in the control. OVAF plus IMHCS showed considerably higher green fluorescence intensity in lysosomes compared to in other groups (control, OVAF, OVAF + CNT, OVAF + QuilA). Moreover,

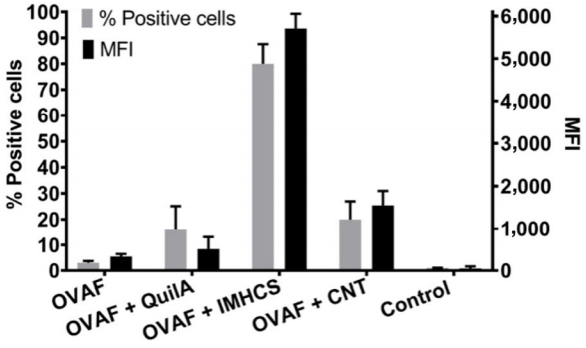

Figure 4 Uptake of OVAF-loaded nanoparticles in RAW 264.7 cells.

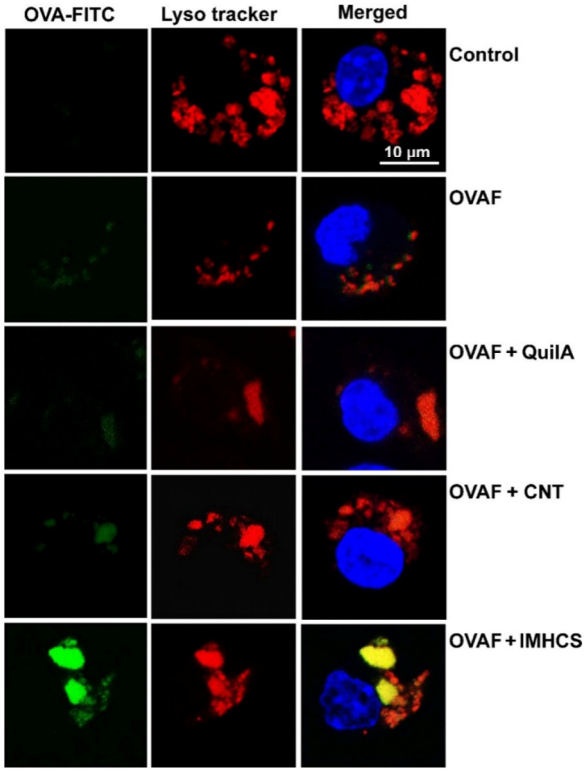

Figure 5 RAW 264.7 cells were incubated with OVA-FITC-loaded nanoparticles for 8 h followed by fluorescent staining of lysosomes using LysoTracker red DND 99 to identify lysosomes (red), nucleus (blue), and OVAF (green).

both green and red fluorescence overlapped to give a yellow color in the merged images for OVAF + IMHCS, indicating that the OVAF did not undergo detectable endo-lysosomal escape. These results indicate that OVA was located in endo-lysosomes, which can cause activation of MHC II marker enhancement and induce a higher antibody response [45].

Matured dendritic cells are the most efficient immunological cells. The maturation of the dendritic cells is characterized by upregulation of surface costimulatory molecules (CD80, CD86, CD40) and various cell surface markers such as MHC II [46, 47]. In this study, the antigens were localized in endosomes; thus, we further tested the activation of MHC II molecules on APCs by conducting a splenocyte maturation test. Splenocytes were isolated from the mouse spleens and studied for maturation after stimulation with OVA, OVA + QuilA, and OVA + IMHCS using FACS *ex vivo*. Because CNT was highly aggregated and showed low OVA loading, high toxicity, and reduced uptake in the APCs, CNT was excluded from the following studies.

As shown in the maturation data obtained from FACS in Fig. 6, the negative control showed no noticeable maturation for MHC II/CD40/CD 80/CD86 in dendritic cells (CD11c-positive) and macrophages (F4/80-positive). In both dendritic cells and macrophages, the cells treated with OVA + IMHCS showed higher expression of MHC II molecules compared to the OVA alone and OVA + QuilA groups. Moreover, CD40 was significantly upregulated. However, there was no significant difference in CD80 and CD86 expression on dendritic cells and macrophages treated with OVA + IMHCS, OVA, and OVA + QuilA.

To study the OVA-specific immune response and adjuvant effect of IMHCS compared with QuilA, C57BL/6J female mice were injected with OVA-loaded IMHCS, pristine OVA, OVA + QuilA, and blank IMHCS. All formulations were prepared on the day of immunization and 3 injections at 3-week intervals were administered. Pre-immune sera and sera at 2 weeks after each injection were collected. All animals remained in healthy conditions throughout the study. Sera collected 14 days after the second boost injection were analyzed for an OVA-specific IgG response by ELISA.

The endpoint titers for the above five groups (including the unimmunized control group) are summarized in Fig. 7(a). The two negative control groups (blank IMHCS and the unimmunized group) showed a negligible immune response compared to the two positive groups (OVA + IMHCS and OVA + QuilA). The pristine OVA group showed a higher response than the two negative groups, but significantly

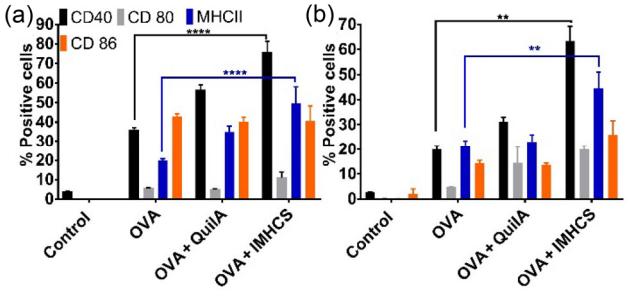

Figure 6 Splenocyte maturation in (a) CD11c-positive dendritic cells and (b) F4/80-positive macrophages. Flow cytometer comparison of maturation markers (CD40, CD80, MHCII, and CD86).

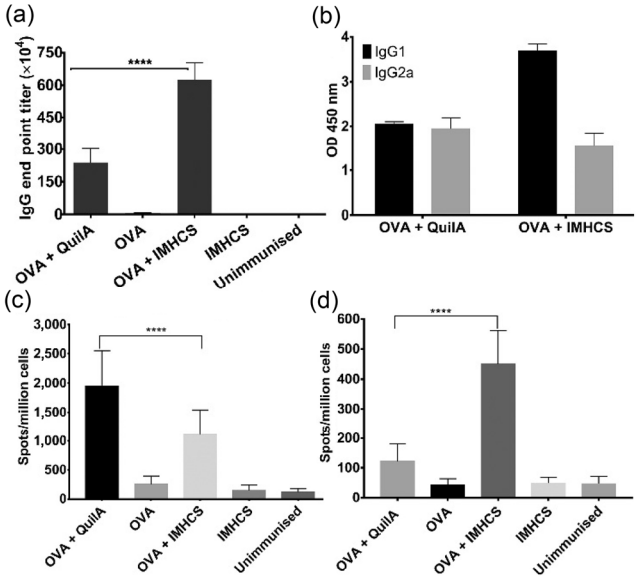

Figure 7 (a) IgG endpoint titer data for 5 groups, (b) OVA-specific IgG antibody isotypes (IgG1 and IgG2a) levels, (c) IFN-γ and (d) IL-4 secretion by splenocytes. Data are expressed as the mean ± S.E.M. (n = 5), *p < 0.05; **p < 0.01; ***p < 0.001; ****p < 0.0001 two way ANOVA test followed by Tukey post-test.

lesser than the two positive groups, suggesting that an adjuvant is required to induce an appreciable immune response. The endpoint titer induced by OVA + IMHCS ($6.24 \times 10^6 \pm 0.78 \times 10^6$) was higher than in the OVA + QuilA group ($2.60 \times 10^6 \pm 0.98 \times 10^6$). This increase may be attributed to the intrinsic hydrophobicity of IMHCS [48], higher antigen uptake, and enhanced maturation of APCs.

Next, to study the nature of the adaptive immune response evoked by the IMHCS, IgG isotypes IgG1 and IgG2a indicative of a Th2- or Th1-biased response were measured in the serum obtained 14 days after the second boost injection of protein [15]. As shown in Fig. 7(b), the ratio of IgG1/IgG2a was close to 1 for the OVA + QuilA group. For the OVA + IMHCS group, the IgG1 concentration was significantly higher (p < 0.0001), while IgG2a was similar compared to the OVA + QuilA group, leading to a higher IgG1/IgG2a ratio (2.00 ± 0.12) and suggesting a Th2-polarized immune response [49]. The increased expression of IgG1 is consistent with the higher activation of CD40 observed in *ex vivo* studies [50]. The other groups showed lower IgG levels, and thus their isotype concentrations were not analyzed.

Cytokines such as IFN-γ and IL-4 are considered to be important mediators in the initiation of cell-mediated and humoral immune responses, respectively [51], and thus IFN-γ and IL-4 levels were further analyzed by the ELISPOT technique. As shown in Fig. 7(c), the concentration of IFN-γ secreted in the OVA + QuilA group was 1,954 ± 435 spots·million^{-1} whereas the OVA + IMHCS group showed a lower IFN-γ concentration of 1,108 ± 594 spots·million^{-1}. Mice administered with pristine OVA showed an even lower IFN-γ concentration of 252 ± 141 spots·million^{-1}. The IFN-γ concentration further decreased to 144 ± 91 and 122 ± 53 spots·million^{-1} in the blank IMHCS and unimmunized groups, respectively. For IL-4 expression (Fig. 7(d)), OVA + IMHCS induced 4-fold higher IL-4 (122 ± 58 spots·million^{-1}) than OVA + QuilA (450 ± 110 spots·million^{-1}), whereas pristine OVA, blank IMHCS, and unimmunized mice showed no significant IL-4 response.

Previous studies suggested that IL-4 expression level is an indicator of the Th2 response [52]. The higher IL-4 response observed in the OVA + IMHCS group compared to the OVA + QuilA group is consistent with the higher IgG1/IgG2a ratio observed in Fig. 7 and higher MHCII expression in the maturation study (Fig. 6), all indicating a Th2-polarized immune response [52]. The high secretion of IL-4 may stimulate B cells to secrete high concentrations of antibodies. This suggests that the Th2-polarized immune response occurs because of the hydrophobic nature of IMHCSs. The intrinsic hydrophobicity of IMHCSs facilitates their accommodation of antigen proteins via the interaction between IMHCSs and hydrophobic regions of proteins. Hydrophobic interactions between IMHCSs and cell membranes also promote high uptake in endo/lysosomes but without effective escape, leading to activation of costimulatory molecules such as MHCII and CD40 and a subsequent Th2-biased immune response.

Other inorganic carriers, typically metal oxides, have been reported as excellent adjuvants for Th2-biased immune responses with strong IgG1 level, including aluminum oxyhydroxide [53] and aluminum silicates [54]. The generation of reactive oxygen species induced by these metal oxides may be responsible for the Th2 immune response [55], which differs from IMHCS. Compared to Quil A, the Th1 immune res-

ponse induced by IMHCSs was lower based on the lower IFN-γ level. However, compared to the OVA group, there was a higher level of IFN-γ, which may maintain the T cell response and sustain the Th1 response [56].

To understand the roles of IMHCSs in the significantly improved IgG and cytokine levels, we conducted *in vitro* analysis of IFN-γ cytokine secretion in RAW 264.7 cells after treatment with OVA-loaded IMHCS (OVA + IMHCS) and physically mixed OVA + IMHCS. As shown in Fig. S7 in the ESM, the cells treated with physically mixed OVA + IMHCS showed a significantly lower IFN-γ secretion level (460 pg·mL^{-1}) than that with OVA + IMHCS (2188 pg·mL^{-1}). However, this level was still much higher than in the negative control group (PBS). These results indicate that both the adjuvant effect and delivery function of IMHCS (sustained release and enhanced uptake) contribute to potent immune responses with improved IgG and cytokine levels in mice, similar to a PLGA nanoparticle system [15].

QuilA is more toxic than IMHCS, which may be related to the immune effect of adjuvants. It has been reported that necrotic cells secrete various damage-associated molecular patterns during the necrosis process, which activate a cascade of immune reactions and consequently drive a Th1 immune response [57, 58]. Thus, the toxicity of QuilA may play a role in Th1 responses. Although IMHCS has a low cellular toxicity and high Th2-biased immune response, their capability in inducing cell-mediated immunity should be improved. Future studies should be devoted to the development of adjuvants with low toxicity and both high Th1 and Th2 immune responses.

4 Conclusions

In conclusion, we explored the adjuvant effect of pristine IMHCSs using OVA protein as a model antigen. IMHCSs exhibited significantly higher loading capacity, more sustained release of OVA, and an improved safety profile compared to most of the studied CNTs. IMHCSs also showed advantages in intracellular delivery of OVA in APCs and splenocyte maturation compared with Quil A. OVA delivered by IMHCSs localized in endosomal/lysosomal compartments in APCs, which may account for the enhanced MHC II activation compared to Quil A. *In vivo* studies revealed that OVA-loaded IMHCSs induced much stronger total IgG responses compared to OVA + QuilA. Higher IgG1 levels than IgG2a suggested a Th2-polarized immune response by IMHCS + OVA, which may be explained by the enhanced endo/lysosome delivery of OVA by IMHCSs. Thus, IMHCSs with a strong antibody response may have potential as an adjuvant for vaccines against infectious bacterial diseases.

Acknowledgements

We thank the support from Australian Research Council, the Australian Microscopy & Microanalysis Research Facility at the Centre for Microscopy and Microanalysis, The University of Queensland, and the Queensland node of the Australian National Fabrication Facility (ANFF). We appreciate the help of Prof. Ian Fraser and Dr. Stacey Cole for the use of ELISPOT reader at Diamantina Institute and Translational Research Institute at The University of Queensland.

Electronic Supplementary Material: Supplementary material (other characterizations and details) is available in the online version of this article at https://doi.org/10.1007/s12274-017-1640-1.

References

[1] Petrovsky, N.; Aguilar, J. C. Vaccine adjuvants: Current state and future trends. *Immunol. Cell Biol.* **2004**, *82*, 488–496.

[2] Marrack, P.; McKee, A. S.; Munks, M. W. Towards an understanding of the adjuvant action of aluminium. *Nat. Rev. Immunol.* **2009**, *9*, 287–293.

[3] Reed, S. G.; Orr, M. T.; Fox, C. B. Key roles of adjuvants in modern vaccines. *Nat. Med.* **2013**, *19*, 1597–1608.

[4] Amanna, I. J.; Slifka, M. K. Contributions of humoral and cellular immunity to vaccine-induced protection in humans. *Virology* **2011**, *411*, 206–215.

[5] Romagnani, S. The Th1/Th2 paradigm. *Immunol. Today* **1997**, *18*, 263–266.

[6] Vogel, F. R.; Powell, M. F. A compendium of vaccine adjuvants and excipients. In *Vaccine Design: The Subunit and Adjuvant Approach*. Powell, M. F.; Newman, M. J., Eds.; Springer: US, 1995; pp 141–228.

[7] Singh, M.; O'Hagan, D. Advances in vaccine adjuvants. *Nat. Biotechnol.* **1999**, *17*, 1075–1081.

[8] Relyveld, E. H.; Bizzini, B.; Gupta, R. K. Rational approaches to reduce adverse reactions in man to vaccines containing tetanus and diphtheria toxoids. *Vaccine* **1998**, *16*, 1016–1023.

[9] Gupta, R. K. Aluminum compounds as vaccine adjuvants. *Adv. Drug Deliv. Rev.* **1998**, *32*, 155–172.

[10] Freund, J.; Casals, J.; Hosmer, E. P. Sensitization and antibody formation after injection of tubercle bacilli and paraffin oil. *Proc. Soc. Exp. Biol. Med.* **1937**, *37*, 509–513.

[11] Zhao, L.; Seth, A.; Wibowo, N.; Zhao, C. X.; Mitter, N.; Yu, C. Z.; Middelberg, A. P. J. Nanoparticle vaccines. *Vaccine* **2014**, *32*, 327–337.

[12] Smith, D. M.; Simon, J. K.; Baker, J. R., Jr. Applications of nanotechnology for immunology. *Nat. Rev. Immunol.* **2013**, *13*, 592–605.

[13] Oyewumi, M. O.; Kumar, A.; Cui, Z. R. Nano-microparticles as immune adjuvants: Correlating particle sizes and the resultant immune responses. *Expert Rev. Vaccines* **2010**, *9*, 1095–1107.

[14] Gregory, A. E.; Titball, R.; Williamson, D. Vaccine delivery using nanoparticles. *Front. Cell. Infect. Microbiol.* **2013**, *3*, 13.

[15] Zhang, W. F.; Wang, L. Y.; Liu, Y.; Chen, X. M.; Liu, Q.; Jia, J. L.; Yang, T. Y.; Qiu, S. H.; Ma, G. H. Immune responses to vaccines involving a combined antigen-nanoparticle mixture and nanoparticle-encapsulated antigen formulation. *Biomaterials* **2014**, *35*, 6086–6097.

[16] Mahony, D.; Cavallaro, A. S.; Stahr, F.; Mahony, T. J.; Qiao, S. Z.; Mitter, N. Mesoporous silica nanoparticles act as a self-adjuvant for ovalbumin model antigen in mice. *Small* **2013**, *9*, 3138–3146.

[17] Yan, S. Y.; Rolfe, B. E.; Zhang, B.; Mohammed, Y. H.; Gu, W. Y.; Xu, Z. P. Polarized immune responses modulated by layered double hydroxides nanoparticle conjugated with CpG. *Biomaterials* **2014**, *35*, 9508–9516.

[18] Wang, T. Y.; Zou, M. J.; Jiang, H. T.; Ji, Z. S.; Gao, P.; Cheng, G. Synthesis of a novel kind of carbon nanoparticle with large mesopores and macropores and its application as an oral vaccine adjuvant. *Eur. J. Pharm. Sci.* **2011**, *44*, 653–659.

[19] Giddam, A. K.; Zaman, M.; Skwarczynski, M.; Toth, I. Liposome-based delivery system for vaccine candidates: Constructing an effective formulation. *Nanomedicine* **2012**, *7*, 1877–1893.

[20] Vasiliev, Y. M. Chitosan-based vaccine adjuvants: Incomplete characterization complicates preclinical and clinical evaluation. *Expert Rev. Vaccines* **2015**, *14*, 37–53.

[21] Tobío, M.; Nolley, J.; Guo, Y. Y.; McIver, J.; Alonso, M. J. A novel system based on a poloxamer/PLGA blend as a tetanus toxoid delivery vehicle. *Pharm. Res.* **1999**, *16*, 682–688.

[22] Dobrovolskaia, M. A.; McNeil, S. E. Immunological properties of engineered nanomaterials: An introduction. In *Handbook of Immunological Properties of Engineered Nanomaterials*. Dobrovolskaia, M. A.; McNeil, S. E., Eds.; World Scientific Publishing Co. Pte. Ltd.: Singapore, 2013; pp 1–23.

[23] Moyano, D. F.; Goldsmith, M.; Solfiell, D. J.; Landesman-Milo, D.; Miranda, O. R.; Peer, D.; Rotello, V. M. Nanoparticle hydrophobicity dictates immune response. *J. Am. Chem. Soc.* **2012**, *134*, 3965–3967.

[24] Kobayashi, K.; Wei, J. J.; Iida, R.; Ijiro, K.; Niikura, K. Surface engineering of nanoparticles for therapeutic applications. *Polym. J.* **2014**, *46*, 460–468.

[25] Bianco, A.; Kostarelos, K.; Partidos, C. D.; Prato, M. Biomedical applications of functionalised carbon nanotubes. *Chem. Commun.* **2005**, 571–577.

[26] Liu, Z.; Tabakman, S.; Welsher, K.; Dai, H. J. Carbon nanotubes in biology and medicine: *In vitro* and *in vivo* detection, imaging and drug delivery. *Nano. Res.* **2009**, *2*, 85–120.

[27] Parra, J.; Abad-Somovilla, A.; Mercader, J. V.; Taton, T. A.; Abad-Fuentes, A. Carbon nanotube-protein carriers enhance size-dependent self-adjuvant antibody response to haptens. *J. Control. Release* **2013**, *170*, 242–251.

[28] Pantarotto, D.; Partidos, C. D.; Graff, R.; Hoebeke, J.; Briand, J. P.; Prato, M.; Bianco, A. Synthesis, structural characterization, and immunological properties of carbon nanotubes functionalized with peptides. *J. Am. Chem. Soc.* **2003**, *125*, 6160–6164.

[29] Kim, T.-W.; Chung, P.-W.; Slowing, I. I.; Tsunoda, M.; Yeung, E. S.; Lin, V. S. Y. Structurally ordered mesoporous carbon nanoparticles as transmembrane delivery vehicle in human cancer cells. *Nano Lett.* **2008**, *8*, 3724–3727.

[30] Wang, J.; Hu, Z. B.; Xu, J. X.; Zhao, Y. L. Therapeutic applications of low-toxicity spherical nanocarbon materials. *NPG Asia Mater.* **2014**, *6*, e84.

[31] Zhang, H. W.; Yu, M. H.; Song, H.; Noonan, O.; Zhang, J.; Yang, Y. N.; Zhou, L.; Yu, C. Z. Self-organized mesostructured hollow carbon nanoparticles via a surfactant-free sequential heterogeneous nucleation pathway. *Chem. Mater.* **2015**, *27*, 6297–6304.

[32] Liu, H. L.; Zhang, Y. L.; Yang, N.; Zhang, Y. X.; Liu, X. Q.; Li, C. G.; Zhao, Y.; Wang, Y. G.; Zhang, G. G.; Yang, P. et al. A functionalized single-walled carbon nanotube-induced autophagic cell death in human lung cells through Akt–TSC2-mTOR signaling. *Cell Death Dis.* **2011**, *2*, e159.

[33] Fang, Y.; Gu, D.; Zou, Y.; Wu, Z. X.; Li, F. Y.; Che, R. C.;

Deng, Y. H.; Tu, B.; Zhao, D. Y. A low-concentration hydrothermal synthesis of biocompatible ordered mesoporous carbon nanospheres with tunable and uniform size. *Angew. Chem., Int. Ed.* **2010**, *49*, 7987–7991.

[34] Demento, S. L.; Cui, W. G.; Criscione, J. M.; Stern, E.; Tulipan, J.; Kaech, S. M.; Fahmy, T. M. Role of sustained antigen release from nanoparticle vaccines in shaping the T cell memory phenotype. *Biomaterials* **2012**, *33*, 4957–4964.

[35] Wang, T. Y.; Jiang, H. T.; Zhao, Q. F.; Wang, S. L.; Zou, M. J.; Cheng, G. Enhanced mucosal and systemic immune responses obtained by porous silica nanoparticles used as an oral vaccine adjuvant: Effect of silica architecture on immunological properties. *Int. J. Pharm.* **2012**, *436*, 351–358.

[36] Musumeci, T.; Ventura, C. A.; Giannone, I.; Ruozi, B.; Montenegro, L.; Pignatello, R.; Puglisi, G. PLA/PLGA nanoparticles for sustained release of docetaxel. *Int. J. Pharm.* **2006**, *325*, 172–179.

[37] Du, J.; Wang, S. T.; You, H.; Zhao, X. S. Understanding the toxicity of carbon nanotubes in the environment is crucial to the control of nanomaterials in producing and processing and the assessment of health risk for human: A review. *Environ. Toxicol. Pharmacol.* **2013**, *36*, 451–462.

[38] Gupta, R. K.; Relyveld, E. H.; Lindblad, E. B.; Bizzini, B.; Ben-Efraim, S.; Gupta, C. K. Adjuvants—A balance between toxicity and adjuvanticity. *Vaccine* **1993**, *11*, 293–306.

[39] Wang, J.; Hu, Z. B.; Xu, J. X.; Zhao, Y. L. Therapeutic applications of low-toxicity spherical nanocarbon materials. *NPG Asia Mater.* **2014**, *6*, e84.

[40] Fiorito, S.; Serafino, A.; Andreola, F.; Togna, A.; Togna, G. Toxicity and biocompatibility of carbon nanoparticles. *J. Nanosci. Nanotechnol.* **2006**, *6*, 591–599.

[41] Wang, C.; Li, P.; Liu, L. L.; Pan, H.; Li, H. C.; Cai, L. T.; Ma, Y. F. Self-adjuvanted nanovaccine for cancer immunotherapy: Role of lysosomal rupture-induced ROS in MHC class I antigen presentation. *Biomaterials* **2016**, *79*, 88–100.

[42] Kalish, R. S. Antigen processing: The gateway to the immune response. *J. Am. Acad. Dermatol.* **1995**, *32*, 640–652.

[43] Vyas, J. M.; Van der Veen, A. G.; Ploegh, H. L. The known unknowns of antigen processing and presentation. *Nat. Rev. Immunol.* **2008**, *8*, 607–618.

[44] Mantegazza, A. R.; Magalhaes, J. G.; Amigorena, S.; Marks, M. S. Presentation of phagocytosed antigens by MHC class I and II. *Traffic* **2013**, *14*, 135–152.

[45] Rafiq, K.; Bergtold, A.; Clynes, R. Immune complex–mediated antigen presentation induces tumor immunity. *J. Clin. Invest.* **2002**, *110*, 71–79.

[46] Gu, L.; Ruff, L. E.; Qin, Z. T.; Corr, M.; Hedrick, S. M.; Sailor, M. J. Multivalent porous silicon nanoparticles enhance the immune activation potency of agonistic CD40 antibody. *Adv. Mater.* **2012**, *24*, 3981–3987.

[47] Yuba, E. Design of pH-sensitive polymer-modified liposomes for antigen delivery and their application in cancer immunotherapy. *Polym. J.* **2016**, *48*, 761–771.

[48] Seong, S. Y.; Matzinger, P. Hydrophobicity: An ancient damage-associated molecular pattern that initiates innate immune responses. *Nat. Rev. Immunol.* **2004**, *4*, 469–478.

[49] Vogel, F. R. Improving vaccine performance with adjuvants. *Clin. Infect. Dis.* **2000**, *30*, S266–S270.

[50] Elgueta, R.; Benson, M. J.; De Vries, V. C.; Wasiuk, A.; Guo, Y. X.; Noelle, R. J. Molecular mechanism and function of CD40/CD40L engagement in the immune system. *Immunol. Rev.* **2009**, *229*, 152–172.

[51] Kaiko, G. E.; Horvat, J. C.; Beagley, K. W.; Hansbro, P. M. Immunological decision-making: How does the immune system decide to mount a helper T-cell response? *Immunology* **2008**, *123*, 326–338.

[52] Vella, A. T.; Dow, S.; Potter, T. A.; Kappler, J.; Marrack, P. Cytokine-induced survival of activated T cells *in vitro* and *in vivo*. *Proc. Natl. Acad. Sci. USA* **1998**, *95*, 3810–3815.

[53] Sun, B. B.; Ji, Z. X.; Liao, Y. P.; Wang, M. Y.; Wang, X.; Dong, J. Y.; Chang, C. H.; Li, R. B.; Zhang, H. Y.; Nel, A. E. et al. Engineering an effective immune adjuvant by designed control of shape and crystallinity of aluminum oxyhydroxide nanoparticles. *ACS Nano* **2013**, *7*, 10834–10849.

[54] Fujimaki, H.; Ozawa, M.; Imai, T.; Kubota, K.; Watanabe, N. Adjuvant effects of aluminum silicate on IgE and IgG1 antibody production in mice. *Int. Arch. Allergy Immunol.* **1984**, *75*, 351–356.

[55] Whitekus, M. J.; Li, N.; Zhang, M.; Wang, M. Y.; Horwitz, M. A.; Nelson, S. K.; Horwitz, L. D.; Brechun, N.; Diaz-Sanchez, D.; Nel, A. E. Thiol antioxidants inhibit the adjuvant effects of aerosolized diesel exhaust particles in a murine model for ovalbumin sensitization. *J. Immunol.* **2002**, *168*, 2560–2567.

[56] Liu, Q.; Jia, J. L.; Yang, T. Y.; Fan, Q. Z.; Wang, L. Y.; Ma, G. H. Pathogen-mimicking polymeric nanoparticles based on dopamine polymerization as vaccines adjuvants induce robust humoral and cellular immune responses. *Small* **2016**, *12*, 1744–1757.

[57] Kono, H.; Rock, K. L. How dying cells alert the immune system to danger. *Nat. Rev. Immunol.* **2008**, *8*, 279–289.

[58] Chung, E. Y.; Kim, S. J.; Ma, X. J. Regulation of cytokine production during phagocytosis of apoptotic cells. *Cell Res.* **2006**, *16*, 154–161.